Emergence of upstream swimming through a hydrodynamic transition

Chih-kuan Tung[1*], Florencia Ardon[2], Anubhab Roy[3], Donald L. Koch[3], Susan S. Suarez[2], and Mingming Wu[1+]

[1] Department of Biological and Environmental Engineering, Cornell University, Ithaca, NY, USA

[2] Department of Biomedical Sciences, Cornell University, Ithaca, NY, USA

[3] School of Chemical and Biomolecular Engineering, Cornell University, Ithaca, NY, USA

E-mail: * ct348@cornell.edu, [+] mw272@cornell.edu

Supplemental Material

A. Theoretical Analysis

A1. Derivation of the dynamic equation for sperm orientation θ

In this section we provide a derivation for the shear-induced rotation of the sperm in Eq. (2) based on the linearity of low Reynolds number flows and the symmetry of the problem. This derivation makes it clear that the rotation results from the local shearing motion near the wall and that the form of the equation is a general result for any axisymmetric but front-back asymmetric object interacting hydrodynamically with a wall. Note that the principle of linear superposition of low Reynolds number flows implies that the rotation of the sperm due to the imposed shear flow can be described independently of the swimming induced rotation provided that one has a specification of the flagellum configuration and we restrict our attention to the former problem here.

To place the result for rotation of a sperm near a wall in context, we first review two related results: (1) the Jeffery rotation of a particle in an unbounded shear flow; and (2) the rotation of a front-back asymmetric particle confined in a channel with a thickness smaller than the particle length. The orientation vector **s** of an axisymmetric particle experiencing a linear flow field far from a wall must be a linear function of the velocity gradient $\nabla\mathbf{u}$ and can depend on the orientation vector **s**. Together with the constraint that **s** remain a unit vector,

$$2s_i\dot{s}_j = \frac{d}{dt}(s^2) = 0.$$

And the requirement that the orientation vector rotate in a solid body rotation when the flow is purely rotational, these observations lead to a rotation rate

$$\dot{s}_i = \mathrm{s_j}\Omega_{\mathrm{ji}} + \lambda\left(\delta_{ij} - s_i s_j\right)E_{jk}s_k, \qquad \text{(S1)}$$

where $\mathbf{\Omega}=(1/2)(\nabla\mathbf{u}-\nabla\mathbf{u}^{\dagger})$ is the rotational and $\mathbf{E}=(1/2)(\nabla\mathbf{u}+\nabla\mathbf{u}^{\dagger})$ the straining portion of the velocity gradient and λ is a rotational parameter whose value depends on the particle geometry. While this equation was first derived by Jeffery [1] for spheroidal particles, Bretherton [2] showed that it applies to all axisymmetric particles. It is noteworthy that the rotation rate predicted by (S1) is antisymmetric upon the transformation $\mathbf{s}\rightarrow-\mathbf{s}$, so that any fixed point for the particle orientation in the upstream

hemisphere of a simple shear flow must have an equivalent fixed point in the downstream hemisphere [2]. It is clear then as noted in Ref. [3] that upstream swimming cannot arise from shear-induced rotation in an unbounded fluid.

If a particle is confined to a channel whose thickness is comparable with the particle length, the particle respond to the full imposed Poisseuille flow in channel, which can be characterized by a mean (gap averaged) velocity **u**. This problem was considered in Ref. [4], for a front-back asymmetric but axisymmetrtic particle. The interest in Ref. [4] was in a microswimmer but the principle of linear superposition implies that the current argument involves only the imposed flow and not the swimming induced motion. In this case, linearity and the maintenance of the unit magnitude of **s** yields:

$$\dot{s}_i = \left(\delta_{ij} - s_i s_j\right) b_j, \qquad \text{(S2)}$$

with

$$b_i = \lambda_1 u_i + \lambda_2 n_i (s_j u_j),$$

where λ_1 and λ_2 can be functions of $\boldsymbol{s}\cdot\boldsymbol{n}$, where $\boldsymbol{n}$ is the unit vector normal to the surface, and we have used the fact that $\boldsymbol{u}\cdot\boldsymbol{n} = 0$ since the surfaces are impermeable. In Ref. [4], it is assumed that $\boldsymbol{s}$ is parallel to the surface as may occur if the length is much larger than the channel thickness and therefore $\boldsymbol{s}\cdot\boldsymbol{n} = 0$, and $\dot{\boldsymbol{s}}\cdot\boldsymbol{n} = 0$. This required $\lambda_2 = 0$ and $\lambda_1 = -\nu$, which must be independent of $\boldsymbol{s}\cdot\boldsymbol{n}$. Thus,

$$\dot{s}_i = -\nu\left(\delta_{ij} - s_i s_j\right) u_j. \qquad \text{(S3)}$$

Please note that we have taken an opposite sign to that appears in Ref. [4]. It is noteworthy that the rotation rate in (S3) unlike that in is an even function of **s** and (S3) can exhibit a stable fixed point in the upstream semi-circle and an unstable fixed point in the downstream semi-circle when $\nu>0$. While the above argument is based solely on linearity and symmetry, it implies that the hydrodynamic interaction of a swimmer with the wall makes a transition to upstream swimming possible.

In the present experiments, the sperm length (about 5 μm) is much smaller than the channel thickness (120 μm). The sperm are observed to swim close to the wall with an orientation that is nearly parallel to the wall. In this situation, the swimmer responds primarily to the local linear flow field near the wall, which is a simple shear flow. While one could use (S3) to describe the present situation, relating the rotation rate to the velocity gradient near the wall has the important advantage that of allowing the result to apply to any channel with a thickness much larger than the swimmer length. It also provides a clearer physical picture of the origin of the rotation.

Thus, we consider a particle orientation vector, which satisfies (S2) to remain a unit vector. In the most general case, the linearity of Stokes flow, $\boldsymbol{b}$ must be linear in $\nabla\boldsymbol{u}$, and can depend on the wall normal **n** and the particle orientation **s**. Thus, **b** can be written as

$$b_i = \lambda_1 n_j \partial_j u_i + \lambda_2 s_j \partial_j u_i + \lambda_3 s_i\left(\partial_j u_j\right) + \lambda_4 n_i s_j\left(\partial_j u_k\right) s_k + \lambda_5 n_i n_j (\partial_j u_k) s_k,$$

where $\lambda_1, \ldots, \lambda_5$ are again functions of $\boldsymbol{s}\cdot\boldsymbol{n}$.

This equation can be simplified using two observations. First, the no slip boundary condition on the wall, a Taylor series expansion for the fluid velocity field and the continuity equation together implies that the velocity gradient must be normal to the wall while the streamlines are locally parallel to

the wall. Thus, the velocity gradient satisfies the constraint

$$\nabla \mathbf{u} = \mathbf{nn} \cdot \nabla \mathbf{u} \cdot (\mathbf{I} - \mathbf{nn})$$

Second, we observe the sperm orientation to be parallel to the wall and thus apply the constraint that $\boldsymbol{s}$ and $\dot{\boldsymbol{s}}$ are perpendicular to $\boldsymbol{n}$, which provides $\boldsymbol{s} \cdot \boldsymbol{n} = 0$ and $\boldsymbol{s} \cdot \boldsymbol{n} = 0$. Using these constraints, it can be shown that $\lambda_2 = \lambda_3 = \lambda_4 = \lambda_5 = 0$, and λ_1 is now independent of $\boldsymbol{s} \cdot \boldsymbol{n}$. Replacing the parameter λ_1 with $-\nu$, we obtain

$$\dot{s}_i = -\nu\big(\delta_{ij} - s_i s_j\big) n_k \partial_k u_j. \qquad \text{(S4)}$$

This form has the advantage of highlighting the relevance of the wall shear rate to the upstream rotation. It should be noted that while both Ref. [4]'s application and ours involve microswimmers, the rotation in Eq. (S3) or (S4) is induced solely by the imposed flow and a similar rotation would occur for a passive front-back asymmetric body. For a front-back symmetric (non-polar) body, one would have the constraint that $\dot{\boldsymbol{s}}$ is invariant to a change of sign of $\boldsymbol{s}$ and this leads to a requirement that $\nu = 0$ so that the flow induced rotation is absent for front-back symmetric bodies.

Given that our swimmers consistently turn to the right in the absence of a flow, equation (S4) is modified as

$$\dot{s}_i = \omega \varepsilon_{ijk} s_j n_k - \nu\big(\delta_{ij} - s_i s_j\big) n_k \frac{\partial u_j}{\partial x_k} \qquad (1)$$

where $\boldsymbol{n}$ is a normal unit vector perpendicular to the surface. Here we have invoked the linear superposition of Stokes flow to superimpose the flow-induced rotation and the swimming induced rotation. We consider $\boldsymbol{s}$ lying with the xy-plane in a Cartesian coordinate system with z perpendicular to the surface so that

$$\boldsymbol{s} = \cos\theta\, \hat{\boldsymbol{x}} + \sin\theta\, \hat{\boldsymbol{y}},$$

and $\nabla \boldsymbol{u} = \hat{\boldsymbol{z}}\hat{\boldsymbol{x}}\gamma$ where γ is the wall shear rate. Thus,

$$\dot{s}_x = -\sin\theta \frac{d\theta}{dt} = \omega \sin\theta + \gamma\nu \sin^2\theta,$$

which yields

$$\frac{d\theta}{dt} = -\omega - \gamma\nu \sin\theta. \qquad (2)$$

A2. Calculation of the rotational parameter ν from the hydrodynamic interaction of a simple model of the microswimmer with the wall

In the previous subsection we used symmetry arguments and the linearity of Stokes flow to demonstrate that Eq. (2) describes the rotation of any axisymmetric swimmer without front-back symmetric which is interacting hydrodynamically with a wall in a shear flow. In this section we will calculate the rotation rate for a specific simple model of a front-back asymmetric swimmer. This calculation will provide a more direct physical picture of the forces and torques that lead to the rotational motion and will also give a crude estimate of the rotational parameter ν.

To study the upstream alignment of a sperm cell in a shear flow we model the cell body as a spherical head of radius a and the flagella as a cylindrical tail of radius r_0 and length $2l$ attached by rigid body constraint to the cell body. The gap-width between the sperm head and wall is h and the sperm cell makes an angle θ with the flow axis (x) and its projection on the vorticity-gradient plane makes an angle ϕ with the vorticity axis (y)

(see SFig. 1). Thus the orientation of the sperm cell is denoted by $\boldsymbol{s} = (\cos\theta\,, \sin\theta\cos\phi,\ \sin\theta\ \sin\phi)$.

The sperm head has a lubrication interaction with the wall, while the flagellar tail modeled with slender-body theory (SBT) has a much weaker hydrodynamic reflection. As a result the mobility of the tail is larger and it is rotated behind the head resulting in upstream orientation. Using a lubrication-SBT composite analysis we will obtain the upstream orientation and calculate the rotation coefficient as a function of shear-rate $(\gamma), l, a, h$ and the aspect ratio of the tail ($\kappa = l/r_0$).

Under the lubrication approximation ($h/a \ll 1$) the forces (F_i^H) and torques (L_i^H) on the sperm head are given by the following resistance matrix formulation,

$$\begin{bmatrix} F_x^H \\ F_y^H \\ F_z^H \\ L_x^H \\ L_y^H \\ L_z^H \end{bmatrix} = \begin{bmatrix} R_{xx}^{FU} & 0 & 0 & 0 & R_{xy}^{F\Omega} & 0 \\ 0 & R_{yy}^{FU} & 0 & -R_{yx}^{F\Omega} & 0 & 0 \\ 0 & 0 & R_{zz}^{FU} & 0 & 0 & 0 \\ 0 & -R_{xy}^{LU} & 0 & R_{xx}^{L\Omega} & 0 & 0 \\ R_{yx}^{LU} & 0 & 0 & 0 & R_{yy}^{L\Omega} & 0 \\ 0 & 0 & 0 & 0 & 0 & R_{zz}^{L\Omega} \end{bmatrix} \begin{bmatrix} U_x \\ U_y \\ U_z \\ \Omega_x \\ \Omega_y \\ \Omega_z \end{bmatrix} + \gamma \begin{bmatrix} R_{xx}^{FS}\, d \\ 0 \\ 0 \\ 0 \\ R_{yx}^{LS} \\ 0 \end{bmatrix}$$

where (U_i, Ω_i) are the translational and angular velocities of the head respectively and $d = h + a$ is the separation of the centre of sperm head from the wall. The resistance matrix helps in calculating the forces and torques from various translational and rotational degrees of freedom [5]. Diagonal terms like R_{xx}^{FU} and $R_{zz}^{L\Omega}$ allow for finding the force in the x direction for uniform translational motion along x and z-torque due to rotation along z-axis. Off-diagonal terms account for coupling of translational and rotational degrees of freedom and arise purely due to hydrodynamic interactions with the wall - $R_{xy}^{F\Omega}$ helps in calculating the drag along x-axis due to a rotation along y-axis. R_{yx}^{LS} and R_{xx}^{FS} are yield the force and torque resulting directly from the imposed shear flow. The leading order form of the various resistivities ($R_{xx}^{FU}, R_{xx}^{L\Omega}, R_{xy}^{F\Omega}, \cdots$) are given as [6,7]

$$R_{xx}^{FU} = R_{yy}^{FU} = -6\pi\mu a\left[\frac{8}{15}\log\left(\frac{a}{h}\right) + 0.96\right]$$

$$R_{zz}^{FU} = -\frac{6\pi\mu a^2}{h}$$

$$R_{xx}^{L\Omega} = R_{yy}^{L\Omega} = -8\pi\mu a^3\left[\frac{2}{5}\log\left(\frac{a}{h}\right) + 0.38\right]$$

$$R_{zz}^{L\Omega} = -8\pi\mu a^3 \times 1.202$$

$$R_{xy}^{LU} = R_{yx}^{LU} = 8\pi\mu a^2\left[\frac{1}{10}\log\left(\frac{a}{h}\right) - 0.19\right]$$

$$R_{xy}^{F\Omega} = R_{yx}^{F\Omega} = 6\pi\mu a^2\left[\frac{2}{15}\log\left(\frac{a}{h}\right) - 0.25\right]$$

$$R_{xx}^{FS} = 6\pi\mu a \times 1.7005$$

$$R_{yx}^{LS} = 4\pi\mu a^3 \times 0.944$$

where μ is the fluid viscosity. The resistivities account for strong hydrodynamic interactions of the cell body with the wall and through a thin lubrication gap. The hydrodynamic interactions of the tail with the wall and the tail with the head are weaker by a factor of at least 1/lnκ, and we ignore these interactions compared with the head-wall interactions; this approximation was used previously by Ref. [8] in a study of bacteria swimming near a wall. This approximation captures the basic physics of upstream rotation which relies on the strong lubrication interaction of the head with the wall which

allows the tail to pivot about the head while being swept downstream.

The tail and head form a rigid body and hence the translational and angular velocities of the tail are ($U_i - (l+a)\epsilon_{ijk}\Omega_j s_k, \Omega_i$) in accordance with the rigid body constraint. From the leading order approximation of SBT, the force per unit length on the tail is given as in Ref. [9],

$$f_i = -\frac{4\pi\mu}{\log 2\kappa}\Big(U_m^T + \epsilon_{mjk}\Omega_j \zeta s_k - u_m^\infty(\zeta \boldsymbol{s})\Big)\Big(\delta_{im} - \frac{1}{2}s_i s_m\Big)$$

where the ambient shear flow is $\boldsymbol{u}^\infty(\zeta \boldsymbol{s}) = \gamma(d + \zeta s_z)\hat{\boldsymbol{x}}$, with $-l \le \zeta \le l$ being the coordinate along the tail. As previously mentioned the translational velocity of the tail is $U_m^T = U_m - (l+a)\epsilon_{mjk}\Omega_j s_k$.

The force and torque acting on the tail are,

$$F_i^T = \int_{-l}^{l} f_i(\zeta)d\zeta = -\frac{4\pi\mu l}{\log 2\kappa}(U_m^T - \gamma d\,\hat{x})(2\delta_{im} - s_i s_m) \quad \text{(S5)}$$

$$L_i^T = \int_{-l}^{l} \epsilon_{ijk}\zeta s_j f_k(\zeta)d\zeta = -\frac{8\pi\mu l^3}{3\log 2\kappa}\big[\Omega_i - s_i\Omega_m s_m + \gamma s_z\big(s_y\hat{z} - s_z\hat{y}\big)\big]$$

For the sperm cell to be force-free and torque-free we combine the lubrication analysis for the sperm head with the SBT calculation for the tail. We thus have

$$F_i^H + F_i^T = 0$$

$$L_i^H + (l+a)\epsilon_{ijk}s_j F_i^H + L_i^T = 0$$

where we have defined the torque relative to the center of the spherical head.

We consider the sperm tail oriented parallel to the wall ($\phi \to 0 \Rightarrow s_z \to 0$) and thus at leading order we need to only consider torque balance in the z direction to calculate the rotation rate from the equation

$$L_3^H + L_3^T + (l+a)\big(s_y F_x^T - s_x F_y^T\big) = 0 \quad \text{(S6)}$$

As $h/a \to 0$, $R_{xx}^{FU}, R_{yy}^{FU}, R_{xy}^{F\Omega}$ and $R_{yx}^{F\Omega}$ diverges as $O(\log(a/h))$ and thus $U_1, U_2 \to 0$. Thus the forces acting on the sperm tail in the flow-vorticity plane, according to SBT (Eq. S5), would be independent of U_i at leading order. We have,

$$F_x^T = -\frac{4\pi\mu l}{\log 2\kappa}\big[2(l+a)\Omega_z s_y - \gamma a(2 - s_x^2)\big] \quad \text{(S7)}$$

$$F_y^T = -\frac{4\pi\mu l}{\log 2\kappa}\big[-2(l+a)\Omega_z s_x + \gamma a s_x s_y\big] \quad \text{(S8)}$$

and substituting (S7) and (S8) in the torque-free condition (S6) we obtain the rotation-rate

$$\Omega_z = \frac{al(l+a)}{1.202\,a^3\log 2\kappa + l^3/3 + l(l+a)^2}\gamma\sin\theta$$

Since $ds_y/dt = \Omega_z s_x$,

$$\frac{d\theta}{dt} = \nu\gamma\sin\theta$$

$$\Rightarrow \theta(t) = 2\cot^{-1}[\exp(c_1 - \nu\gamma t)]$$

where

$$\nu = \frac{al(l+a)}{1.202\,a^3\log 2\kappa + l^3/3 + l(l+a)^2}$$

is the rotation coefficient.

Thus for long times, $\theta(t \to \infty) \to \pi$ denoting upstream alignment of the sperm cell. To obtain a characteristic value of the rotation coefficient we need to consider realistic values for l, a and κ. The bull sperm studied in experiments has a paddle-shape

head, with approximate dimensions of 10 μm long, 5 μm wide, and roughly 1 μm thick. The head is directly connected to a single flagellum that is about 50 - 60 μm long and tapers from 1 μm in diameter at the connection to 200 nm at the tail end. We consider the paddle-shaped head to be a triaxial ellipsoid and we choose the spherical head in the theoretical model to have the same surface area so that they have comparable resistance - a 5.16 μm spherical head. Thus for a $50-60\ \mu m$ tail of 1 μm cross-section size the rotation coefficient obtained theoretically varies as $\nu \approx 0.0731-0.0616$. The experimentally observed value of ν is 0.118 ± 0.005 . Without using any fitting parameters we have thus obtained comparable values for the rotation coefficient by using a very simple model for sperm cell. Our model captures the essential physics necessary for upstream alignment –the cell body having a strong lubrication interaction with the wall and the flagella pivoting about the head due to the imposed shear flow and being rotated downstream.

A3. Solving the Fokker-Planck equation

Fokker Planck equation provides us with

$$\frac{\partial p}{\partial t} = -\frac{\partial}{\partial \theta}\left(\dot{\theta} p\right) + \frac{\partial}{\partial \theta} D_r \frac{\partial p}{\partial \theta}, \qquad \text{(S9)}$$

where $p(\theta)$ is the probability distribution of the sperm head orientation θ , D_r is the rotational diffusion coefficient of the microswimmer, and $\dot{\theta}$ is described in equation (2). The relative contribution of the circling motion and the angular fluctuation to sperm swimming dynamics is determined by a Péclet number, $\mathrm{Pe} = \omega/D_r$. In our experimental situation, the measured Pe = 3.1.

At steady state $\partial \mathrm{p}/\,\partial \mathrm{t} = 0$, equation (S9) provides

$$\frac{\partial}{\partial \theta}\left(D_r \frac{\partial p}{\partial \theta} - \dot{\theta} p\right) = 0,$$

therefore

$$D_r \frac{dp}{d\theta} - (-\omega - \gamma\nu \sin\theta) p = C. \qquad \text{(S10)}$$

Equation (S5) is a first-order differential equation with integrating factor

$$\mu = e^{\int \frac{1}{D_r}(\omega + \gamma\nu \sin\theta) d\theta},$$

and

$$p(\theta) = \frac{\int \mu \frac{C}{D_r} d\theta'}{\mu} = e^{-\int_0^\theta \frac{1}{D_r}(\omega+\gamma\nu \sin\theta\prime) d\theta'} \left[\int_0^\theta e^{\int_0^{\theta'} \frac{1}{D_r}(\omega+\gamma} \quad \text{(S11)}$$

$$+ C_2\Big].$$

We next numerically integrate

$$I_2 = e^{-\int_0^\theta \frac{1}{D_r}(\omega+\gamma\nu \sin\theta\prime) d\theta'}$$

and

$$I_1 = e^{-\int_0^\theta \frac{1}{D_r}(\omega+\gamma\nu \sin\theta\prime) d\theta\prime} \left[\int_0^\theta e^{\int_0^{\theta\prime} \frac{1}{D_r}(\omega+\gamma\nu \sin\theta") d\theta"} d\theta'\right]$$

separately, with $\Delta\theta$ step size is 0.01 rad, as $p(\theta) = C_1 I_1 + C_2 I_2$. The ratio of $\mathrm{C}_1/\mathrm{C}_2$ was next determined by the periodic boundary condition, $p(0) = p(2\pi)$, and then the magnitude of the constants determined by the normalization $\int_0^{2\pi} p(\theta) d\theta = 1$.

A4. Langevin simulation

In Langevin simulation, the dynamics equation (2) can be written as

$$\frac{d\theta}{dt} = (-\omega - \gamma\nu \sin\theta) + \xi', \qquad \text{(S12)}$$

where ξ' is a random number that corresponds to the rotational diffusivity. To solve the stochastic dynamic equation (S12), the time evolution of θ follows

$$\theta_{i+1} - \theta_i = -\omega \triangle t - \gamma\nu \sin\theta_i \triangle t + \xi, \qquad \text{(S13)}$$

where ξ is a random number chosen between [-0.088942,0.088942]. This range is consistent with $\sqrt{2D_r\Delta t}X$, where X is a random number with a unit standard deviation. The initial $\theta_{t=0}$ was chosen randomly between $[0,2\pi]$. The range of ξ was confirmed by diffusion coefficient calculated from 400 traces of random walks $\Delta\theta = \xi$. Δt time step is 0.0112 s. In SFig. 5, it can be shown that the Langevin simulation using this ξ range yields results comparable to Fokker-Planck calculation. 400 traces were simulated using equation (S13) for 1 min, and the last θ were used to calculate $\langle s_x \rangle$.

To understand the discrepancy of the predicted transition curve from Fokker-Planck equation and the experimental value, we took into account the wiggling motion of the sperm due to the beating of the flagellum using the Laugevin model. The wiggling of the sperm head is measured with an amplitude A = 0.45 rad and frequency f = 18.6 Hz. We then used a sinusoidal function to approximate the wiggling, therefore

$$\frac{d\theta}{dt} = (-\omega - \gamma\nu \sin\theta) + 2\pi f A \cos 2\pi f t.$$

For each step Δt,

$$\theta_{i+1} - \theta_i = (-\omega - \gamma\nu \sin\theta)\triangle t + 2\pi f A \cos 2\pi f t \ \triangle t + \xi, \qquad \text{(S14)}$$

where ξ is the same random number uniformly chosen between [-0.088942,0.088942], and the initial condition $\theta_{t=0}$ was randomly chosen between [0, 2π]. The solution is shown as dashed line in Fig. 4(a).

B. Discussion

B1. Brief summary of the comparison of our work with that of Kantsler *et al.* (2014) (Ref. [3] here or Ref. [7] in the main text)

The experiments and theory of Ref. [3] like those in our Letter show that sperm can swim upstream in an imposed flow field. However, there are two important insights that our work provides that are not elucidated in Ref. [3]. First, by considering the competition between the circling swimming motion of the cells and the rotation induced by the flow, we have identified experimentally and theoretically a critical shear rate needed for upstream swimming to occur. The theory of Ref. [3] considered the rotational swimming to be random and did not lead to a transition from circling to directed upstream swimming. Second, the physical mechanism for the flow-induced rotation of the cells was not clearly explained in Ref. [3] and this omission made it unclear how general the result would be. In the text of the Ref. [3], this rotation is discussed in terms of the collision of a cell with the wall. However, in the supplemental materials, it is noted that such a collision for a simple model of a swimmer that rotates in the Jeffery rotation for an axisymmetric particle in the absence of a wall does not lead to a net rotation toward the upstream direction. The authors then developed in the supplemental material a detailed model considered a spiral flagellum with the origin of the spiral constrained to be at a fixed point on the wall. No physical mechanism was mentioned for the constraint placed on the flagellum's origin. The resultant calculation leads to a rotation rate of the form of Eq. (2) in the limit of a tight spiral where chiral effects are small. Our derivations clarify the critical role of the cell-wall hydrodynamic

interaction in creating upstream rotation. It also demonstrates that the hydrodynamically induced rotation occurs for any front-back asymmetric body interacting hydrodynamically with a wall and thereby shows that upstream swimming would be a general phenomenon.

In addition, the hydrodynamic bifurcation theory proposed here (and the resulting scaling law and onset point) is important for the following two reasons: (i) it provides a simple and robust mechanism for explaining upstream swimming behavior. Adler equation proposed here links the problem of upstream swimmer to a large class of problem. All front-back asymmetric microswimmers that swim near surface and in circles will swim upstream. (ii) From biological side, it elucidates the importance of criticality in regulating biological function. Previously, it has been suggested that biological systems are fine-tuned by evolution to operate near critical transition points in order to optimize sensitivity to changes in environmental stimuli [10]. However, this is the first time that fluid flow is suggested as a driving force to regulate micro-swimmers at a critical point.

By reading Ref. [3] carefully, using data from 1 mPa s medium and human sperm data for example, we found that their lowest flow shear rate is 1.07 ± 0.06 1/s. Further, in 1 mPa s medium, human sperm have mean radius of curvature of 1790 ± 415 μm and average speed of 54 ± 3 μm/s, which provide ω = 0.030 ± 0.007 rad/s. According to our theory, assuming the two share similar ν, this provides γ_c = 0.24 ± 0.06 1/s, which is significantly smaller than the minimal flow shear (1.07 1/s) they applied in the 1 mPa s medium. Since they did not provide curvature data for their bull sperm, we are not able to calculate the corresponding critical shear for their experiment.

In low viscosity fluid, the right hand chiral trajectories observed in our work and those of Ref. [3] are similar. In high viscosity fluid, Ref. [3] reported a mean left hand chiral trajectory, which is consistent with our observation as well as current literature [11]. In this case, sperm uses a very different swimming strategy, they swim via the planar beating of the flagellum (instead of self-rolling as in the case of low viscosity fluid) [11,12]. It has been established that a sperm sample consists two subpopulations with opposite handedness [12-15]. The right hand chiral swimmers are found to be more motile in low viscous medium, and the left hand ones are more motile in high viscous medium [For detailed discussions, please see Ref. [12]. The exact mechanism for these two different motility patterns remains unknown. This is a very interesting question, and it is an ongoing research project of our lab.

B2. An orientation disorder-to-order transition

In addition to the emergence of sperm upstream swimming, there is also an orientational disorder-to-order transition, in which the orientation of the sperm head changes from random to alignment with respect to each other. Here we define an order parameter, s_a , which is the absolute value of $\langle \boldsymbol{s} \rangle$, for the measure of the orientation 'orderliness' of the swimming pattern. $s_a = 0$ when sperm heads are orientated randomly; and $s_a = 1$ when all sperm heads are pointing to one direction, regardless of the swimming direction with respect to the flow. A similar order parameter has been defined in a work on phase transition in a system of self-driven particles [16], and serves as a nonequilibrium analogue of the ferromagnetic (XY) model in equilibrium system [17]. A power law of close to 0.5 is also found to be true for s_a

versus $\gamma - \gamma_c$ (see SFig. 7). Please note that the angle of the order phase is not spontaneously chosen, but follows θ_0 as described in SFig. 7.

C. Materials and Methods

C1. Microfluidic device fabrication

The microfluidic device was fabricated using standard soft lithography technique. The silicon master was first made using a deep silicon etching process, and the final microfluidic device was replicated from the silicon master using the PDMS stamping technique.

The fabrication of the negative silicon master mould was done at Cornell NanoScale Science & Technology Facility (CNF). Deep silicon etching steps were masked by thick photoresist to achieve the 120 μm deep main channel. The detailed procedures were as follows: photoresist (Megaposit SPR2 20-7.0, Shipley, Marlborough, MA, USA) was then spun onto a 100 mm silicon wafer (SEMI standard, SSP, 0.5 mm thick) (2500 rpm for 40 s), soft baked at 115 °C for one min, and then exposed (1.05 J/cm^2) on a contact aligner (Karl Suss MA/BA 6 aligner, Suss MicroTec, Garching, Germany, soft contact mode). The resist was developed 90 min after the exposure. After developing the resist (60 s AZ 726 MIF development, HamaTech-Steag Wafer Processor, Santa Clara, CA, USA), the wafer was then etched by a Botsch deep silicon etching process (Unaxis 770 Deep Silicon Etcher, Oerlikon, Pfäffikon, Switzerland) for 120 μm. The resist was removed by two steps, first immersing the wafer in a hot bath (Resist Hot Strip Bath, with propylene glycol, NMP, TMAH heated at 60°C) for 90 min, followed by a 90 s oxygen plasma ashing (AURA 1000 Resist Strip, GaSonics, San Jose, CA, USA), since some resist might have been hardened in the DRIE process. After the thorough stripping processes, the wafer was next treated with (*1H,1H,2H,2H*-Perfluorooctyl) Trichlorosilane, or FOTS, using a single layer vapour deposition method (Molecular Vapor Deposition, Applied Microstructures, San Jose, CA, USA) to ensure the easy release of PDMS from the silicon master.

We next prepared the PDMS piece, and bonded it onto a PDMS coated glass slide. 9:1 base to curing agent PDMS (SYLGARD 184 Silicone Elastomer Kit, Dow Corning, Midland, MI, USA) procedures were used for making a PDMS replica from the silicon master, and a PDMS coated glass slide from a flat glass surface. After curing, one 2 mm hole and one 1 mm hole were punched using biopsy punches (Miltex Inc, York, PA, USA), in order to provide access to the channels. The PDMS piece and the PDMS coated glass slide were next treated with oxygen plasma for one min on a high power setting using a plasma cleaner (Harrick Plasma Cleaner PDC-001, Harrick Plasma, Ithaca, NY, USA). The PDMS device was next sandwiched between a Plexiglas manifold and the PDMS coated glass slide for 10 min to ensure the quality of bonding, with the PDMS coated side touching the structured side of the PDMS device. The bonded device was then released from the Plexiglas manifold, and tubing (Weico Wire & Cable, ETT-24, Edgewood, NY, USA) was inserted into the 1 mm hole to provide a flow. The assembly was next wetted with de-ionized water, and autoclaved immersed in DI water to ensure sterile conditions, and remove air bubbles.

C2. Flow control and measurement

Fluid flows within the microfluidic channels were generated by a syringe pump (KDS-230, KD Scientific, Holliston, MA, USA), and 1 mL syringes (BD, Franklin Lakes, NJ, USA). The flows were measured using a particle tracking method with 0.51 μm diameter fluorescent beads (Dragon Green, Bangs Laboratories, Fishers, IN, USA). Images of the fluorescent beads were taken with short exposure time (10 ms) at 30 frames/s with flow rates ranging from 0-5 μL/min. We then tracked each bead's location over time to obtain the flow speeds.

Since the spatial resolution of particle tracking is limited by the optical resolution of the microscope, especially in the *z* direction, we used COMSOL Multiphysics 4.3 to obtain finer structures of the flow profiles, and compared with the experimental measurements. The Navier-Stokes Equation was solved to calculate the flow field using a 3D laminar flow model.

C3. Imaging and data analysis

Sperm images were taken by a NEO sCMOS camera (DC-152Q-C00-FI, Andor Technology, Belfast, UK) in conjunction with an inverted phase contrast microscope (Axiovert 35, Carl Zeiss Microscopy, Thornwood, NY, USA) with a 10X objective. The images were recorded using NIS Elements software (Nikon Instruments, Inc., Melville, NY, USA). For motility and orientation analysis, the sperm were tracked using ImageJ. A "Manual Cell Tracking" add-on was used for tracking, and the trajectories were analysed using GraphPad Prism and an in house MATLAB program. Lines were drawn from tails to heads for the orientation analysis, and the angles were measured by ImageJ. To avoid over sampling the same cells, images were analysed with 3 s intervals, and all cells in the given frame were analysed until the total count exceeds 400.

The swimming speed of sperm was computed using the displacement of the sperm between consecutive images (sampled at 8.17 Hz) and divided by time.

C4. Reagents and media

Chemicals used in this segment were purchased from Sigma-Aldrich unless otherwise noted. Tyrode Albumin Lactate Pyruvate (TALP) [18], a modified Tyrode balanced salt solution, was used as sperm medium. TALP consisted of 99 mM NaCl, 3.1 mM KCl, 25 mM $NaHCO_3$, 0.39 mM NaH_2PO_4, 10 mM HEPES free acid, 2 mM $CaCl_2$, 1.1 mM $MgCl_2$, 25.4 mM sodium lactate, 0.11 mg/mL sodium pyruvate, 5 μg/mL gentamicin, and 6 mg/mL bovine serum albumin (Fraction V; Calbiochem, La Jolla, CA, USA), with a pH of 7.4 and 300 mOsm/kg. TALP was equilibrated in a 38.5 °C incubator with 5% CO_2 in humidified air before use.

C5. Bull sperm sample preparation

Semen samples frozen in plastic straws were kindly provided by Genex Cooperative, Inc. (Ithaca, NY, USA). The straws had been diluted in egg yolk extender and frozen according to the standard procedures followed at Genex Cooperative, Inc., which are described in Ref. [19] Procedures to prepare the sperm from the frozen samples are described in Ref. [20] Briefly, the straws were first thawed in a 37°C water bath, and then seminal plasma, extender, and dead

sperm were removed from live sperm by density gradient centrifugation (300 x g for 10 min) through two layers (40-80%) of BoviPure diluted in BoviDilute (Spectrum Technologies, Inc., Healdsburg, CA, USA). The sperm pellet was then washed in 3 mL TALP (300 x g, 3 min). Sperm were resuspended in 20 μL of TALP, and kept in an incubator at 38.5 °C under 5% CO_2 in humidified air until used. Sperm concentration was determined using an improved Neubauer hemacytometer and adjusted to 10^8 cells/mL.

C6. Experimental setup

Prior to running the experiments, the devices were flushed with TALP medium to remove the water in the system. The devices were then submerged under TALP, and equilibrated in a 38.5 °C incubator with 5% CO_2 in humidified air overnight. During the experiments, the microfluidic devices were kept at 38.5 °C by a temperature-controlled thermal plate (H401-T-BL-LOG, OkoLab, Ottaviano, NA, Italy) and heated stage (TRZ 3700, Carl Zeiss). Sperm suspensions were seeded through the 2 mm hole on the device, and sperm were allowed to swim in with no flow applied. A sperm concentration suitable for the experiments was established in the centre area within 3-5 min. Next, different flow rates were applied in the experiments, and we compared sperm behaviours on flat surfaces with behaviours in the microgrooves. We waited 1 min before the video acquisition to ensure the stabilization of the flow. A typical experiment lasted 1.5-2 hr.

C7. Measurements of circling frequency ω and rotational diffusion coefficient D_r

The circling angular frequency ω and the rotational diffusion coefficient D_r used to solve equation (S9 and S12) are determined by the experiments as shown in SFig. 4. In SFig. 4(a)-(c), we have 50 traces of $\theta(t)$ - $\theta(0)$ versus time at different flow rates. Clearly, sperm orientation display a random fluctuation superimposed on a CW circling motion. We therefore fitted the angular mean squared displacement (MSD) to $\omega^2 t^2 + 2D_r t$. The fitted parameters provide the values of the rotational diffusion coefficient D_r and sperm circling angular frequency ω as shown in SFigs. 4 (e) and (f). The sperm rotational diffusion coefficient remain nearly constant for all the flow rates tested. However, the sperm circling frequency dropped significantly at the onset of upstream swimming. For the theoretical analysis, D_r and ω were taken from the no flow measurements.

C8. Measurements of wiggling frequency f and amplitude A

The wiggling motion of the sperm was characterized using video taken at 200 FPS. The number of frames of each period of wiggling was recorded, and then converted to frequency. The amplitude was measured as the difference between the maximum and minimum angle θ within one period. Results are shown in SFig. 6.

D. Movies

SMovie 1 Sperm motility with a CCW self-rotation. Sperm roll in a CCW direction

when viewed from the front. Video was recorded at 200 FPS, and replayed at 10 FPS. Scale bar: 20 μm.

SMovie 2 Sperm swim in circular trajectories when there was no flow. Video was recorded at 7.12 FPS, and replayed at 7 FPS. Scale bar: 100 μm.

SMovie 3 Sperm hits a side wall and stays along the side wall. Video was recorded at 100 FPS, and replayed at 10 FPS. Scale bar: 20 μm.

SMovie 4 Sperm swim along a side wall. Video was recorded at 200 FPS, and replayed at 10 FPS. Scale bar: 20 μm.

SMovie 5 Sperm swim in linear trajectories when their orientations were locked by an above critical flow ($\gamma = 6.4$ 1/s) toward the left. When their orientations were not at the preferred orientations, they were reoriented into the preferred orientation. Video was recorded at 7.12 FPS, and replayed at 7 FPS. Scale bar: 100 μm.

E. Supplemental Figures

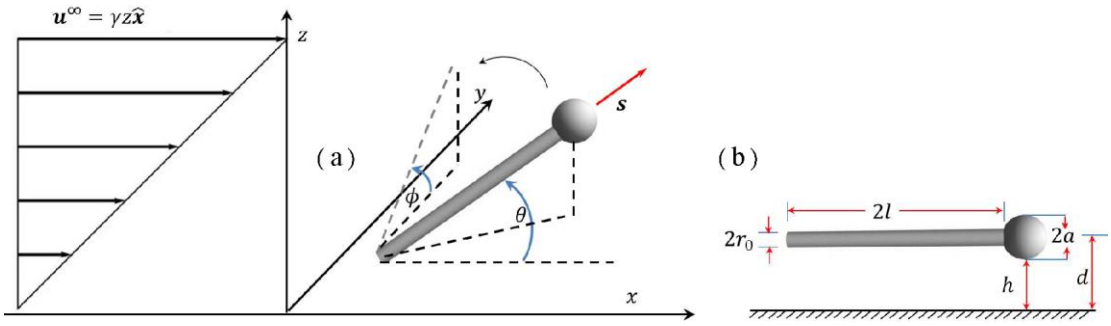

SFIG. 1 Schematic of the theoretical model for upstream swimming of sperm cell.

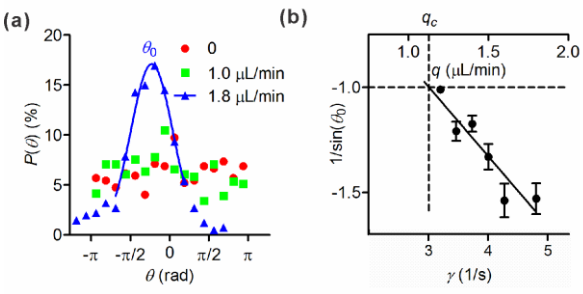

SFIG. 2 Determination of q_c. (a) θ_0 only emerges when $q > q_c$. (b) q_c is determined by linear fit of $1/\sin\theta_0$.

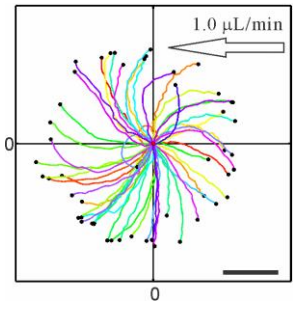

SFIG. 3 Sperm trajectories exhibit similar curvatures under a flow that has a shear rate

less than the critical shear rate. Scale bar: 100 μm.

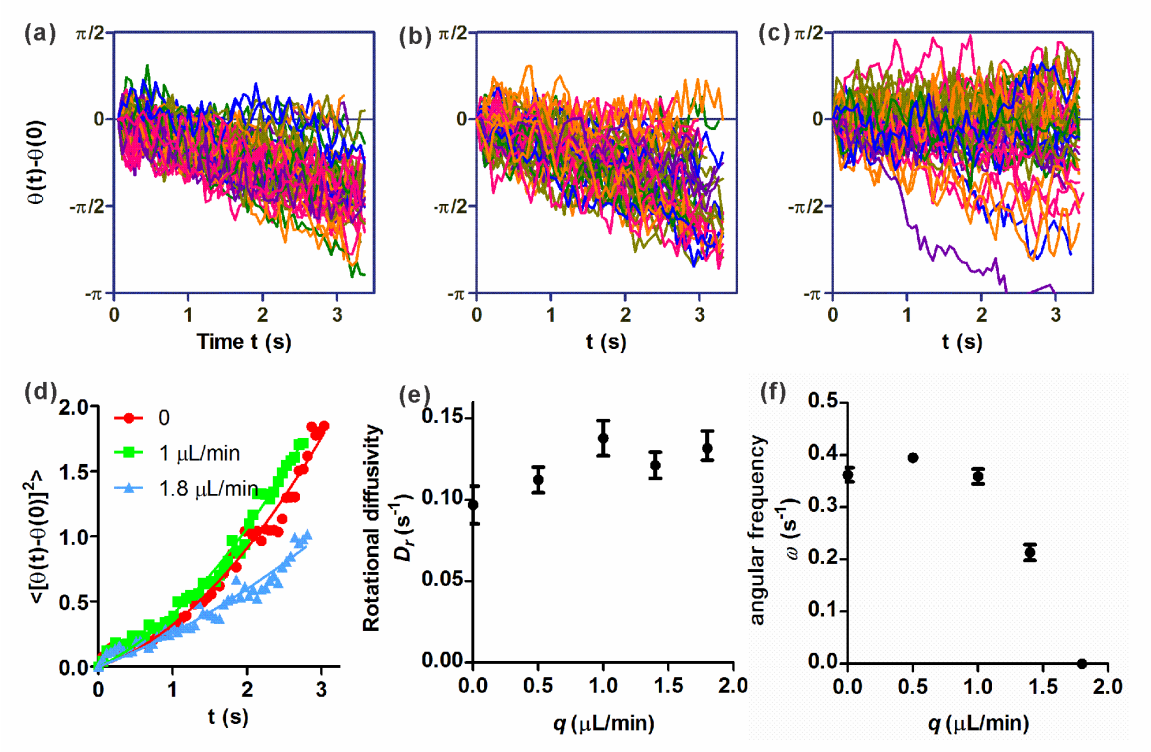

SFIG. 4 Circling sperm with rotational diffusion. (a)-(c) Time evolution of sperm swimming orientation $\theta(t) - \theta(0)$ in the absence of a flow (a), below critical flow rate (b), and above critical flow rate (c). 50 sperm tracks are depicted here. (d)-(f) Angular mean squared displacements $\langle[\theta(t) - \theta(0)]^2\rangle$ versus time at three flow rates. Solid lines are fits to $\omega^2 t^2 + 2D_r t$, where ω is the sperm circling frequency and D_r is the rotational diffusivity coefficient. The fitted D_r is shown in (e) and ω in (f) for various flow rates. $\omega = 0.36 \pm 0.01$ rad/s at no flow.

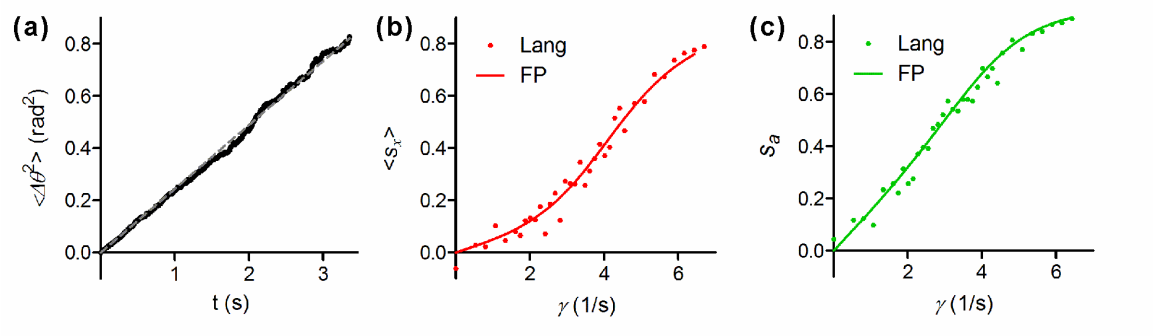

SFIG. 5 Validation of ξ in the Langevin model. (a) Angular mean squared displacement (MSD) of a random walk $\Delta\theta = \xi$ yields a diffusion coefficient of 0.122, similar to the experimentally measured value of 0.120. (b)-(c) For both $\langle s_x \rangle$ (b) and s_a (c) the Langevin simulations with $A = 0$ reproduced the results from solving Fokker-Planck model.

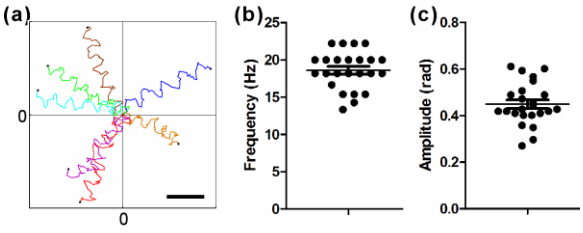

SFIG. 6 Measurements of the wiggling motion of sperm migration. (a) Tracking high frame rate videos of sperm movement shows the wiggling motion. The videos were recorded and tracked at 200 FPS, and all tracks shown are 0.35 s long. Scale bar: 20 μm. (b)-(c) The frequency of the wiggling is found to be 18.6 ± 0.5 Hz, and the amplitude 0.45 ± 0.02 rad. Measurements taken from 200 FPS videos.

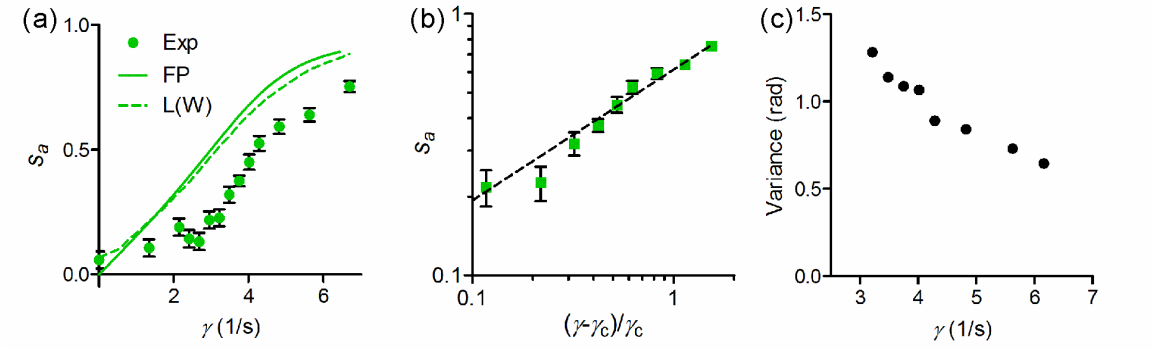

SFIG. 7 An orientation disorder-order transition. (a) Experimentally measured $s_a = \|\langle \boldsymbol{s} \rangle\|$ also shows significant increase after an onset. (b) s_a also scales with $\gamma - \gamma_c$ as a power law with an exponent 0.51 ± 0.03. (c) Another way to see the emergence of the overall order in orientation is the sharper Gaussian curves seen in SFig. 2. Variance, or the standard deviation measured from the Gaussian fits, decreases as γ increases, resulting in increasing overall orderliness at higher flow.

Supplemental References

[1] G. B. Jeffery, Proc. R. Soc. A **102**, 161 (1922).

[2] F. P. Bretherton, J. Fluid Mech. **14**, 284 (1962).

[3] V. Kantsler, J. Dunkel, M. Blayney, and R. E. Goldstein, eLife **3**, e02403 (2014).

[4] T. Brotto, J.-B. Caussin, E. Lauga, and D. Bartolo, Phys. Rev. Lett. **110**, 038101 (2013).

[5] J. Happel and H. Brenner, *Low Reynolds Number Hydrodynamics: With Special Applications to Particulate Media* (Springer Netherlands, 1983), Vol. 1.

[6] A. J. Goldman, R. G. Cox, and H. Brenner, Chem. Eng. Sci. **22**, 637 (1967).

[7] A. J. Goldman, R. G. Cox, and H. Brenner, Chem. Eng. Sci. **22**, 653 (1967).

[8] E. Lauga, W. R. DiLuzio, G. M. Whitesides, and H. A. Stone, Biophys. J. **90**, 400 (2006).

[9] G. K. Batchelor, J. Fluid Mech. **44**, 419 (1970).

[10] O. Kinouchi and M. Copelli, Nature Phys **2**, 348 (2006).

[11] B. M. Friedrich, I. H. Riedel-Kruse, J. Howard, and F. Jülicher, J. Exp. Biol. **213**, 1226 (2010).

[12] D. F. Babcock, P. M. Wandernoth, and G. Wennemuth, BMC Biol. **12**, 67 (2014).

[13] S. Ishijima, M. S. Hamaguchi, M. Naruse, S. A. Ishijima, and Y. Hamaguchi, J. Exp. Biol. **163**, 15 (1992).

[14] T.-W. Su, L. Xue, and A. Ozcan, Proc. Natl. Acad. Sci. USA **109**, 16018 (2012).

[15] T.-W. Su, I. Choi, J. Feng, K. Huang, E. McLeod, and A. Ozcan, Sci. Rep. **3**, 1664 (2013).

[16] T. Vicsek, A. Czirók, E. Ben-Jacob, I. Cohen, and O. Shochet, Phys. Rev. Lett. **75**, 1226 (1995).

[17] P. M. Chaikin and T. C. Lubensky, *Principles of Condensed Matter Physics* (Cambridge University Press, 2000).

[18] J. J. Parrish, J. Susko-Parrish, M. A. Winer, and N. L. First, Biol. Reprod. **38**, 1171 (1988).

[19] M. T. Kaproth, H. E. Rycroft, G. R. Gilbert, G. Abdel-Azim, B. F. Putnam, S. A. Schnell, R. W. Everett, and J. E. Parks, Theriogenology **63**, 2535 (2005).

[20] F. Ardon and S. S. Suarez, Reproduction **146**, 111 (2013).